SUPPLEMENTARY INFORMATION

doi:10.1038/nature11025

Contents:

I. INTRODUCTION

In this supplementary information we give a full theoretical background of the gating of ionization and recombination times presented in the paper, and describe in detail our analysis methods. In section II we describe the experimental methods. In section III we present the semi-classical equations describing the displacement and velocity gates, and show how we use them for retrieving the ionization and recollision times for each harmonic order. Section IV describes how we extract the relevant parameters for the displacement and velocity gates out of the experimental two-color delay scan. In section V we discuss the case of two-channel ionization, and its effect on the gated signal. Next, we give an extended theoretical overview of various aspects of our work. In section VI we derive a full quantum description of the displacement gate. We consider the effect of the weak second harmonic field on the initial velocity and displacement, as well as the effect of the core potential on the perturbation. We show that these effects give minor corrections to the semi-classical gate. In section VII we discuss the role of the measurement in strong field dynamics, and the comparison between HHG and other strong field processes. Finally, in section VIII we discuss the implication of our measurement on possible definitions of the ionization time.

II. EXPERIMENTAL METHODS

High harmonics are generated with 30 fs, 1 kHz, 800 nm laser pulses focused into a 100 Hz pulsed gas jet. The pulse intensity is estimated according to the cutoff harmonic as 3.8×10^{14} W/cm^2 in the helium experiment (Fig. 3a,b) and 1.3×10^{14} W/cm^2 in the CO_2 experiment. The second harmonic (SH) field, on a 1(2) percent intensity level in the helium (CO_2) experiment, is produced using a 100 μm type-I BBO (BaB_2O_4) crystal. The SH field is orthogonally polarized with respect to the fundamental field. Group-velocity dispersion is compensated using a birefringent crystal (calcite). The sub-cycle delay ϕ of the SH field relative to the fundamental field is controlled by rotating 1 (0.5) mm of fused silica in the helium (CO_2) experiment. High harmonics are generated by focusing the two color beam into a pulsed gas jet (backing pressure 3 atm) using a curved mirror (f = 75 cm). The harmonic spectrum is measured by an XUV spectrometer. For the molecular alignment, the laser pulse is split into pump (alignment) and probe (generating) pulses, which are focused non-collinearly in the gas jet, see Fig. 1 (SI). The generating arm includes the two-color setup described above. A motorized stage in the pump arm controls the delay between the alignment pulse ($I \sim 3.5 \times 10^{13}$ W/cm^2) and the two-color pulse. The polarization of the alignment pulse is set by using a zero order half wave plate. An additional 0.5 mm of fused silica is placed in the alignment arm and rotated by the same angle as in the generating arm in order to keep the delay between the pump and probe pulses constant.

III. TEMPORAL CHARACTERIZATION USING TWO-COLOR GATES

We generate two independent sub-cycle gates by adding a weak cross-polarized second harmonic (SH) field to the fundamental field. The perturbative nature of the second field is essential, greatly simplifying further analysis.

First, it ensures that the times of ionization and recombination t_i and t_r are dictated by the longitudinal dynamics in the strong fundamental field and in the field of the ionic core, but remain unaffected by the weak SH field. Second, the effect of the Coulomb potential of the ion on the motion induced by the perturbing field is negligible. Analysis in Sec. VI shows that, due to the large value of the amplitude of electron oscillations in the strong fundamental field, the effect of the ionic potential is almost decoupled from the lateral motion induced

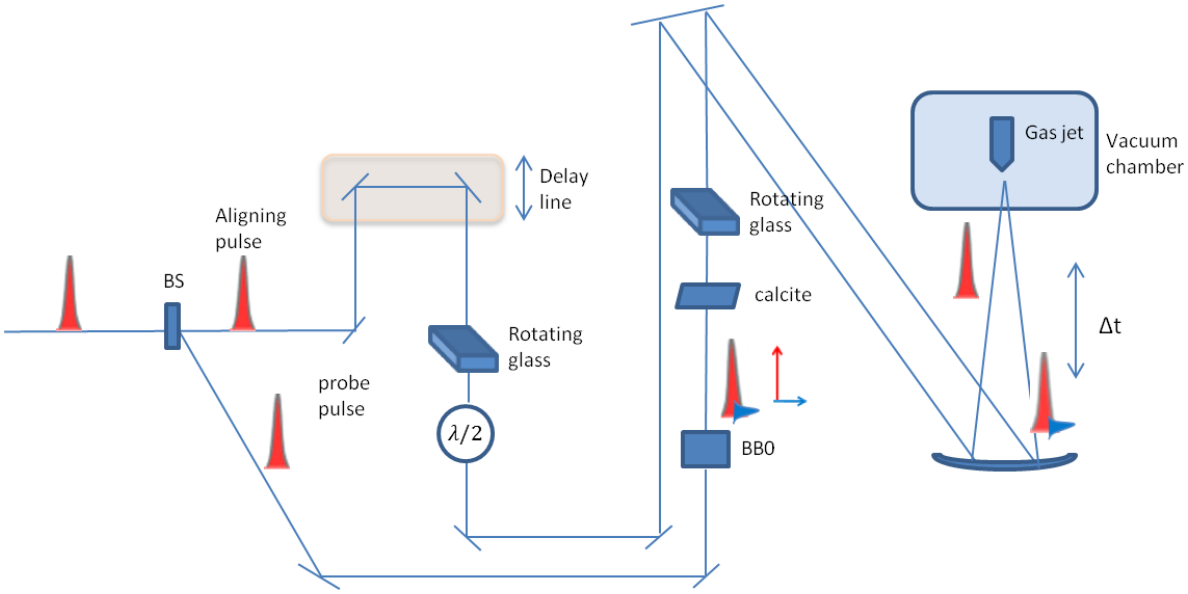

FIG. 1: Schematic description of the experimental setup.

by the perturbative field, with the relevant small parameter less than $I_p/(16U_p) \ll 1$.

With these two aspects in mind, consider first the semi-classical analysis of the effect of the second field, with the fully quantum treatment deferred to Sec. VI. The key assumption of the semi-classical analysis is to neglect the effect of the weak SH field during electron tunneling, and to include only the lateral motion induced after ionization. The validity of this assumption is checked in Sec. VI which contains the full quantum treatment, but the comparison of the two approaches is shown already in this section, justifying the semi-classical treatment.

A. The displacement gate.

Neglecting the effect of the weak field on tunneling, the condition for zero lateral displacement of the electron between ionization and recombination reads

$$\int_{t_i}^{t_r} (v_{0y} - A_{2\omega}(t_i) + A_{2\omega}(t''))dt'' = 0. \quad (1)$$

Here v_{0y} is the lateral electron velocity at the moment of ionization t_i, $A_{2\omega}(t)$ is the vector-potential for the SH field polarized along the y-axis, $F_y = F_{2\omega}\cos(2\omega t + \phi)$. The field amplitude is $F_{2\omega} = \epsilon F_0$ with $\epsilon \ll 1$, and ϕ controls the two-color delay. Solving the above

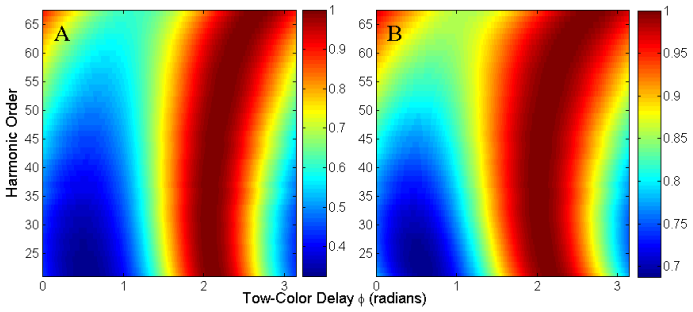

FIG. 2: Comparison of the displacement gate $[G_y(\phi)]^2$ calculated using:. A. Full quantum analysis. B. Semi-classical calculation.

equation, we find the initial electron velocity v_{0y} at time t_i required for recombination at t_r. This velocity compensates for the lateral displacement induced by the SH field:

$$v_{0y}(t_r, t_i, \phi) = -\epsilon \frac{F_0}{2\omega} \left[\sin(2\omega t_i + \phi) + \frac{\cos(2\omega t_r + \phi) - \cos(2\omega t_i + \phi)}{2\omega(t_r - t_i)} \right]. \tag{2}$$

As confirmed by previous measurements, which studied the effect of the fundamental field's ellipticity of the harmonics emission [1], the dependence of the tunnelling amplitude on the initial lateral velocity v_{0y} is [2] $\exp(-v_{0y}^2 \tau_T/2)$, where τ_T is the so-called tunnelling time – the imaginary part of $t_0 = t_i + i\tau_T$. Thus, the expression for the displacement gate is

$$G_y(t_r, t_i, \phi) = e^{-\frac{1}{2} v_{0y}^2(t_r, t_i, \phi)\tau_T}. \tag{3}$$

Note, that τ_T determines the contrast of the gate's modulation. However, our reconstruction procedure relies solely on the *phase* of the oscillations, and therefore is independent of the value of τ_T. Figures 2a, b in the article illustrate the gate which suppresses the harmonic yield according to the electron dynamics along the lateral direction – dictated by both t_r and t_i.

Figure 2 (SI) compares the semi-classical displacement gate (B) given by Eq.(3) with the results of the fully quantum analysis (A), described in Sec. VI. The gates are shown for the conditions of our experiment in helium. The figure demonstrates excellent agreement between the optimal two-color delay derived from the simple semi-classical analysis and the full quantum treatment.

B. The velocity gate.

The second gate is induced by the lateral *velocity* of the free electron at the moment of recombination t_r, v_y. It is related to v_{0y} as $v_y = v_{0y} - A_{2\omega}(t_i) + A_{2\omega}(t_r)$. Substituting the optimal velocity given by Eq.(2) for v_{0y} yields the associated velocity v_y at the moment of recombination, which defines the velocity gate:

$$G_v(t_r, t_i, \phi) = \frac{v_y(t_r, t_i, \phi)}{v_x(t_r, t_i, \phi)} = \frac{\epsilon F_0/2\omega}{\sqrt{2(N\omega - I_p)}} \left[\sin(2\omega t_r + \phi) + \frac{\cos(2\omega t_r + \phi) - \cos(2\omega t_i + \phi)}{2\omega(t_r - t_i)} \right] \quad (4)$$

where the energy of the longitudinal motion $E(t_r)$ is given by the emitted harmonic photon energy $N\omega$, $E(t_r) = N\omega - I_p$.

Whereas the displacement gate is mapped onto the HHG intensity, the lateral recombination velocity – the velocity gate – dictates the vectorial properties of the emitted light and is mapped into the HHG polarization state (Fig. 2c and d in the article).

The two gates induced by the two-color configuration satisfy three key requirements for optimal sub-cycle gates. First, they are perturbative, probing the interaction without modifying its basic properties. We verified this by comparing the experimental results for two different intensities of the SH, taken at 1% and 2% intensity level of the fundamental field. The dependence of the harmonic intensity on the two-color delay was found to be the same for both intensities. Thus, for our experimental conditions, the SH field does not affect the reconstruction of the ionization and recombination times (see Sec. VI).

Second, for most trajectories the displacement gate G_y changes rapidly with the ionization time, whereas the velocity gate G_v changes rapidly with the recollision time. Indeed, for sufficiently long travel times $(t_r - t_i)$, the first term in square brackets in Eq.(2) and in Eq.(4), dominates. In this limit, the displacement gate depends mostly on t_i, and the velocity gate depends mostly on t_r. For very low harmonics each gate is sensitive to both t_i and t_r; this dependence is of course taken into account in our calculation.

Third, the two gates are symmetric under translations in t_i (for G_y) or t_r (for G_v) and we can easily shift the gates within the optical cycle by controlling the relative phase ϕ between the two colors.

In summary, our two color configuration inherently induces two independent gates which depend on the lateral displacement and lateral velocity. Experimentally, we can decouple their contribution. The displacement gate G_y is measured for each harmonic number by

measuring the signal intensity whereas the velocity gate G_v is measured by resolving the harmonics polarization state. Both observables - intensity and polarization - are modified with ϕ. They impose a set of two equations for every harmonic order. Solving these equations we can extract both the ionization time t_i and the recombination time t_r for each harmonic order.

C. Reconstruction of t_i and t_r.

We analyzed the attenuation profile of each harmonic order as a function of the phase between the fields ϕ, related to the displacement gate G_y and the polarization angle as a function of ϕ, related to the velocity gate G_v (see details in Sec. IV). For each case we used a fitting procedure to find $\phi^y_{max}(N)$, the phase for which the harmonic signal is maximal and $\phi^v_{max}(N)$, the phase that maximizes the harmonic polarization angle. For each harmonic order, ϕ^y_{max} and ϕ^v_{max} enforce the gating equations:

$$\frac{\partial G_y(t_r,t_i,\phi)}{\partial\phi}\,|_{\phi^y_{max}}=0, \quad \frac{\partial G_v(t_r,t_i,\phi)}{\partial\phi}\,|_{\phi^v_{max}}=0, \tag{5}$$

these are two equations with two unknown variables: t_i and t_r. The reconstructed ionization and recombination times which solve these equations are shown in Fig. 3c in the article.

An important parameter which is not directly measured in our experiment is the absolute phase between the two fields (ϕ). A shift in this phase would cause an absolute shift of the total reconstructed curve of $t_i(N)$ and $t_r(N)$, but without changing the time delay between ionization and recollision, or between different harmonics. In order to fix this phase we rely on the recombination times measurement. We fit the absolute phase such that the deviation: $|t_r^{rec}(N) - t_r^{theory}(N)|$, averaged over N, is minimized (t_r^{rec}: reconstructed times, t_r^{theory}: stationary solution times). Such fitting optimizes the absolute position of t_r^{rec}, whereas the slope is directly determined by our experimental measurement. The shaded area represents the experimental uncertainty which originates from the uncertainty in the determination of the cutoff. This shifts the absolute phase between the fields such that an error of $\pm$4.5 eV in the cutoff creates a shift of $\pm$25 asec in the reconstructed times.

IV. HHG INDUCED BY A TWO-COLOR FIELD IN THE MULTI-CYCLE REGIME

In the previous section we analyzed the gating mechanism induced by a single half cycle of the fundamental field. Our experiment is performed in the multicycle regime, therefore the interference between attosecond pulses generated by adjacent half cycles has to be analyzed. The following analysis relies on the study of HHG with a two-color field applied to probe the structure of atomic wavefunctions [3]. When HHG is induced by a two-color field, both odd and even harmonics are generated. The orthogonal configuration controls both the displacement of the electron from the parent ion and the recollision angle, as described in the previous section. In this section we will show how the multicycle configuration allows us to extract these two characteristics.

The motion of the free electron along the fundamental field's polarization is inverted between consecutive half-cycles of the field, whereas the motion along the second harmonic (SH) field's polarization axis does not change. This difference breaks the symmetry of the process and gives rise to even harmonic orders polarized along the SH polarization axis ($\mathbf{e}_y$) whereas odd harmonics are polarized along the fundamental polarization ($\mathbf{e}_x$). A detailed analysis of the free electron's dynamics is provided in [4].

Next, we consider the recollision stage of HHG. When the free electron recollides with the ion it is spread in space and appears as a wave traversing the ion at a certain angle dictated by the electron's trajectory. During recollision a dipole moment is induced, leading to the emission of optical radiation. When the bound state is spherically symmetric (as in helium), the dipole oscillates along the recollision axis, leading to the emission of harmonics polarized along this angle. The odd and even harmonic spectra are projections of the total spectrum on the polarization axes of the fundamental and SH field, respectively. Their intensities are described as:

$$I_{odd}(N\omega) = I(N\omega)\cos^2(\theta), \quad I_{even}(N\omega) = I(N\omega)\sin^2(\theta), \tag{6}$$

where N represents the harmonic order and θ is the angle between the recollision axis and the x axis. As described in Sec. III two main parameters are manipulated in our experiment: the lateral displacement and the lateral velocity. The lateral displacement dictates the total signal intensity $I(N\omega) \propto G_y^2$ whereas the lateral velocity dictates the

recollision angle according to: $\tan\theta = v_y/v_x$, where v_y and v_x are the lateral and longitudinal velocities, respectively. In the perturbative regime v_x is not modified, therefore θ reflects the modification of v_y.

If we assume that the dipole moment is smooth as a function of energy, we can decouple the two gates. The sum of consecutive harmonics will cancel the dependence on the recollision angle and will enable us to extract $I(N\omega)$ and therefore the displacement gate G_y. The ratio of consecutive harmonics is $I_{even}(N\omega)/I_{odd}(N\omega) \simeq \tan^2(\theta) = G_v^2$. This calculation normalizes the dependence on the signal intensity and directly extracts the recollision angle θ and the velocity gate G_v.

V. TWO-COLOR GATING OF TWO IONIZATION CHANNELS

For two ionization channels contributing to the harmonic emission, the total signal is the coherent sum of the two channel contributions. In the absence of the weak second-color field,

$$S_N = S_N^{(1)} + S_N^{(2)} + 2\sqrt{S_N^{(1)} S_N^{(2)}} \cos\Delta\varphi_N. \tag{7}$$

Here $S_N^{(i)}$ is the harmonic intensity for channel i and $\Delta\varphi_N$ is the relative phase between the two channels, which varies with the harmonic order N. When the weak gating field $F_{2\omega}$ is added, the signal becomes

$$\widetilde{S}_N(\phi) = S_N^{(1)} G_N^{(1)}(\phi)^2 + S_N^{(2)} G_N^{(2)}(\phi)^2 + 2\sqrt{S_N^{(1)} S_N^{(2)}} G_N^{(1)} G_N^{(2)} \cos\Delta\varphi_N, \tag{8}$$

with $G_N^{(i)}(\phi)$ the two-color (displacement) gates for the harmonic amplitudes and ϕ the two-color delay. In principle, the two gates are complex-valued. Small differences between the two channels imply that the relative phase φ_N can be modified by the difference between the phases of the two gates. However, for a weak field $F_{2\omega}$ this difference and the corresponding change of φ_N is negligible. Thus, the assumption of purely amplitude modulation is justified by the perturbative nature of the gate.

For channels with close I_p's, there are only small differences in the ionization and recombination times and hence the corresponding gates $G_N^{(i)}(\phi)$ are very close. Thus, we can introduce the average gate $G_N(\phi)$ and the difference $\Delta G_N(\phi)$:

$$\Delta G_N = G_N^{(1)} - G_N^{(2)}$$

$$G_N = \frac{G_N^{(1)} + G_N^{(2)}}{2}$$
$$G_N^{(1)} = G_N + \frac{1}{2}\Delta G_N$$
$$G_N^{(2)} = G_N - \frac{1}{2}\Delta G_N \tag{9}$$

Substituting these expressions into Eq.(8) and dropping the terms quadratic in ΔG_N, we obtain

$$\widetilde{S}_N(\phi) = G_N^2(\phi) S_N \left[1 + \frac{\Delta G_N(\phi)}{G_N(\phi)} \times \frac{S_N^{(1)} - S_N^{(2)}}{S_N}\right]. \tag{10}$$

Analyzing this expression, one can see that for constructive interference, where $S_N = \left(\sqrt{S_N^{(1)}} + \sqrt{S_N^{(2)}}\right)^2$, the second term is negligible relative to the first. Therefore, the average gate, which is very similar to $G_N^{(1)}$ and $G_N^{(2)}$, is measured. However, for destructive interference $S_N = \left(\sqrt{S_N^{(1)}} - \sqrt{S_N^{(2)}}\right)^2$ and the second term becomes large. In this case the quadratic terms in ΔG_N cannot be neglected since the leading terms become small due to the destructive interference. The full expression is almost similar:

$$\widetilde{S}_N(\phi) = G_N^2(\phi) S_N \left[1 + \frac{1}{2}\frac{\Delta G_N(\phi)}{G_N(\phi)} \times \frac{\sqrt{S_N^{(1)}} + \sqrt{S_N^{(2)}}}{\sqrt{S_N^{(1)}} - \sqrt{S_N^{(2)}}}\right]^2, \tag{11}$$

and clearly shows that the destructive interference between the two ionization channels leads to a major contribution of the differential gate ΔG_N. Next, we derive an expression for $\Delta G_N(\phi)$ and explain why the contribution of the differential gate leads to a phase jump.

For the weak SH field the displacement gates $G_N^{(i)}(\phi)$ have the following form:

$$G_N^{(i)}(\phi) = a_N^{(i)} + b_N^{(i)} \cos[2(\phi - \phi_N^{(i)})]. \tag{12}$$

Here $a_N \simeq 1 - b_N$ determines the average signal level, $b_N \ll 1$ is the modulation depth, and ϕ_N is the optimal two-color delay. Equation (12) does not contain any higher harmonics of the two-color delay ϕ, which is appropriate for the perturbative regime. The gate described in Eq.(12) reflects a π-periodicity of the modulation as a function of the two-color delay ϕ, confirmed by our experiments. This periodicity follows from the π- periodicity of the harmonic generation response to the total field $F_\omega \cos(\omega t) + F_{2\omega} \cos(2\omega t + \phi)$ if the medium is mirror-symmetric with respect to the polarization of the fundamental field. This is the case for both atoms and aligned but not oriented molecules.

We denote:

$$\begin{aligned} a_N^{(1)} &= a_N + \frac{1}{2}\Delta a_N \ , \ a_N^{(2)} = a_N - \frac{1}{2}\Delta a_N \\ b_N^{(1)} &= b_N - \frac{1}{2}\Delta b_N \ , \ b_N^{(2)} = b_N + \frac{1}{2}\Delta b_N \\ \phi_N^{(1)} &= \phi_N + \frac{1}{2}\Delta \phi_N \ , \ \phi_N^{(2)} = \phi_N - \frac{1}{2}\Delta \phi_N \end{aligned} \tag{13}$$

Substituting these notations in Eq.(12) and neglecting all terms quadratic in the small difference $\Delta\phi$ between the two gates, for the differential gate we find

$$\Delta G_N = \Delta a_N - \Delta b_N \cos[2(\phi - \phi_N)] + 2b_N \Delta\phi_N \sin[2(\phi - \phi_N)]. \tag{14}$$

Introducing the angle θ_N

$$\tan\theta_N = \frac{2b_N\Delta\phi_N}{\Delta b_N}, \tag{15}$$

we re-write the differential gate as

$$\Delta G_N(\phi) = \Delta a_N + \Delta b_N \sqrt{1 + \left(\frac{2b_N\Delta\phi_N}{\Delta b_N}\right)^2} \cos\left[2\left(\phi - \phi_N + \frac{\pi}{2} + \frac{\theta_N}{2}\right)\right]. \tag{16}$$

This expression allows one to easily characterize the phase-shifts in the gated harmonic signal as a function of the two-color delay ϕ.

Let us now analyze the experimental results presented in Fig.4 in the article, according to the above expressions. In CO_2 molecules both the HOMO and HOMO-2 orbitals contribute to the signal. In the low harmonic orders the signal from the HOMO dominates, and therefore phase of the maximal signal is the same for 90 and 0 degrees of alignment (contributions only from HOMO, or from both HOMO and HOMO-2 respectively). Consider now the vicinity of the destructive interference between the two channels, where both orbitals give comparable contributions. The two-color gates for these orbitals are very close, in agreement with our assumptions above for small ΔG.

According to Eqs. (11, 16), as long as $\Delta S \equiv \sqrt{S_N^{(1)}} - \sqrt{S_N^{(2)}}$ is small enought, or if Δa_N, Δb_N and ΔS all have the same sign, then the differential signal maximizes when

$$\phi = \phi_N - \frac{\pi}{2} - \frac{\theta_N}{2}. \tag{17}$$

Analysis of the gate shows that for short trajectories (which are the ones measured in our experiment) the angle θ remains quite small. This yields around $\pi/2$ phase shift of the

gated signal. This can be observed in the phase jump of the harmonic signal around the destructive minimum in 0° alignment.

Indeed, for short trajectories the gate parameter a_N increases with N and hence with the electron travel time in the continuum $t_r - t_i$, whereas the modulation depth b_N decreases with N. Since for a deeper orbital the travel time is shorter for the same N, the parameter a_N is slightly larger for HOMO than for HOMO-2, while b_N is slightly larger for HOMO-2. Therefore, both Δa_N and Δb_N are positive. As long as the signal from channel 1 (HOMO in the case of CO_2) is larger than that from channel 2 (HOMO-2 for the CO_2 molecule), the differential signal maximizes when $\Delta G_N(\phi)$ has maximum, which corresponds to $\phi \sim \phi_N - \frac{\pi}{2}$. Near the cutoff, the signal from the deeper orbital often dominates, which means that the optimal two-color delay would now correspond to the minimum of the differential gate:

$$\phi = \phi_N - \pi - \frac{\theta_N}{2} \quad , \text{or} \quad \phi = \phi_N - \frac{\theta_N}{2}. \tag{18}$$

Since in the cutoff ϕ_N becomes N-independent, $\theta_N \simeq 0$, we see that the optimal delay either makes the overall π-jump compared to the optimal delays before the destructive interference of the two channels,

$$\phi \simeq \phi_N - \pi, \tag{19}$$

or returns back to the original single-channel branch

$$\phi = \phi_N. \tag{20}$$

Due to the π-periodicity, the two branches are, of course, equivalent. Which of the two looks to be a smoother continuation of the initial jump depends on fine details of the N-dependence of ϕ_N and θ_N. A small displacement beyond $\pi/2$ in Eq.(17) means that the branch Eq.(19) might look like a more natural continuation.

VI. QUANTUM DESCRIPTION OF HARMONIC EMISSION IN A TWO-COLOR FIELD

A. Two-color gating of harmonic emission and the effects of the core potential

Here we give a quantum description and show how the weak control (SH) field at the frequency 2ω perturbs (gates) the harmonic signal, including the effect of the Coulomb potential on the perturbation (gate).

Let us begin with the standard analysis which relies on the strong-field approximation (SFA), where the induced dipole moment at the frequency Ω can be written as:

$$\mathbf{d}(\Omega) = -i \int dt \int dt' \int d\mathbf{p} C(\mathbf{p}, t, t') e^{-iS(\mathbf{p},t,t') - iI_p(t-t') + i\Omega t}. \tag{21}$$

Here t is associated with the moment of recombination, t' with the moment of the bound-free transition, $\mathbf{p}$ is the drift (canonical) momentum of the electron and the amplitude $C(\mathbf{p}, t, t')$ includes the recombination amplitude at t, the propagation amplitude between t' and t, and the amplitude of the bound-free transition at t'. The phase $S(\mathbf{p}, t, t')$

$$S(\mathbf{p}, t, t') = \frac{1}{2} \int_{t'}^{t} dt'' \left[\mathbf{p} + \mathbf{A}(t'')\right]^2 \tag{22}$$

is the energy-related component of the classical action, with $\mathbf{A}$ the vector-potential of the laser field. These equations can be viewed as the application of the Feynman path formalism to the harmonic generation problem [5].

The so-called quantum orbits are the trajectories along which the phase of the multi-dimensional integral Eq.(21) is stationary. They are obtained by differentiating this phase with respect to the integration variables $\mathbf{p}$, t', and t, yielding correspondingly:

$$\begin{aligned} &\int_{t'}^{t} [\mathbf{p} + \mathbf{A}(t')] dt' = 0, \\ &\frac{[\mathbf{p} + \mathbf{A}(t')]^2}{2} + I_p = 0 \\ &\frac{[\mathbf{p} + \mathbf{A}(t)]^2}{2} + I_p = \Omega \ . \end{aligned} \tag{23}$$

We will denote instants t and t' which solve these equations as t_r and t_0 correspondingly.

Whereas the SFA provides excellent *qualitative* description of the harmonic emission, it is generally not sufficient for quantitative analysis. The latter requires one to include the effect of the core potential. The way to incorporate the corresponding corrections was proposed in Ref.[6] and improved and thoroughly investigated in [7–9]. The corrections use Eqs. (23) as a zero-order approximation.

To achieve quantitative accuracy, one has to first replace the plane-wave recombination amplitude which enters $C(\mathbf{p}, t, t')$ by the accurate recombination amplitude. This amplitude is obtained using correct continuum states at the electron energy corresponding to the energy of the emitted photon, i.e. to the kinetic momenta corresponding to the instantaneous kinetic momentum $\mathbf{p} + \mathbf{A}(t)$ at the moment of recombination t in Eqs.(23).

Further, the core potential $U(r)$ has to be included into the action. The correction can be done in the eikonal approximation, which allows one to obtain a reliable description of ionization[10] and of the interplay between the core potential and the laser field (the so-called Coulomb-laser coupling[11–14]) during the electron propagation after ionization. The phase in Eq.(22) becomes [12, 15]

$$S(\mathbf{p}, t, t') = \frac{1}{2}\int_{t'}^{t} dt'' \left[\mathbf{p} + \mathbf{A}(t'')\right]^2 + \int_{t'}^{t} dt'' U(\mathbf{r}_0(t'')). \tag{24}$$

The second integral is performed along the zero-order (SFA) trajectory, which starts near the core at the moment t' and returns to its original position at t:

$$\mathbf{r}_0(t) = \int_{t'}^{t} dt''[\mathbf{p} + \mathbf{A}(t'')] + \mathbf{r}_{\text{in}} \tag{25}$$

The starting position $\mathbf{r}_{\text{in}}$ of the trajectory is uniquely defined from the asymptotic behavior of the ionizing state, yielding $r_{\text{in}} = 1/\sqrt{2I_p}$ [10]. For complex values of $t' = t_0 = t_i + i\tau$, which realize the stationary phase of the multi-dimensional integral Eq.(21), the integral from $t' = t_0$ to the real time axis determines the tunnel ionization amplitude, and the contribution of the core potential to the integral provides the required Coulomb correction to the ionization rate [10]. The resulting amplitude yields excellent agreement with ab-initio numerical simulations of strong-field ionization (see e.g. [16–18]) for a broad range of frequencies and Keldysh parameters γ. Correction to the ionization amplitude included in the so-called quantitative rescattering model [7] effectively incorporates the same procedure by re-normalizing the results to the correct ionization rates.

Using the Coulomb-corrected expression Eq.(24), we are in a position to analyze how the weak control SH field 2ω, polarized along the y axis, perturbs the phase of the integral Eq.(21). First, it changes the kinetic energy term in Eq.(24) by adding $A_{2\omega}(t)$ orthogonally polarized to $A_\omega(t)$ and the lateral momentum $\mathbf{p}_y$. Second, the SH field introduces a lateral displacement $\Delta\mathbf{r}$ of the zero-order trajectory $\mathbf{r}_0$ into the integral from $U(\mathbf{r})$. The phase accumulated along the stationary trajectory becomes

$$S(\mathbf{p}, t, t') = \frac{1}{2}\int_{t'}^{t} dt'' \left[(p_x + A_\omega(t''))^2 + (p_y + A_{2\omega}(t''))^2\right] + \int_{t'}^{t} dt'' U[\mathbf{r}_0(t'') + \Delta\mathbf{r}(t'')]. \tag{26}$$

Note that corrections to $t = t_r$ and $t' = t_0$ enter in higher orders thanks to the stationary conditions Eqs.(23). Furthermore, the first-order correction in the expansion of the core potential in $\Delta\mathbf{r}(\tau)$ is equal to zero because the scalar product $\mathbf{r}_0(\tau) \cdot \Delta\mathbf{r}(\tau) = 0$. Thus, in

leading order with respect to $A_{2\omega}$ the change in the action is:

$$\Delta S(p_y, t_r, t_0) = \frac{1}{2}\int_{t_0}^{t_r} dt'' \left[[p_y + A_{2\omega}(t'')]^2 - \frac{Q}{|r_0(t'')|}\frac{[\Delta x(t'')]^2}{r_0^2(t'')} \right] \tag{27}$$

Here we have substituted the Coulomb potential $U(r) = -Q/r$ and took into account that $\Delta\mathbf{r}$ is parallel to the y axis, denoting $\Delta r = \Delta y$. Note that Δy is linear in p_y and $A_{2\omega}$, and hence the second term is quadratic in the weak field.

Let us now analyze the two terms in the integrand in Eq.(27). Note that $t_0 = t_i + i\tau$ is complex. The integral is performed along the contour which first descends from the complex t_0 to the real time axis, and then continues to t_r. The part of the integral between t_0 and the real time axis is related to ionization. The first term in the integrand in Eq.(27) corrects the ionization amplitude due to the change in the external field. This correction remains in the exponent. The correction to the ionization amplitude coming from the second term will correspond to the modifications of the pre-exponential Coulomb correction to the SFA-based ionization rate. It is therefore small compared to the exponential corrections.

Moreover, the lateral drift momentum $p_y^{(ion)}$ which optimizes *ionization* will correspond to the trajectory for which

$$\frac{\partial}{\partial p_y}\Delta S(p_y, t_i, t_0) = 0. \tag{28}$$

This condition means zero lateral displacement of the tunnelling trajectory at the moment when it emerges from the tunnelling barrier. As expected, tunnelling introduces exponential penalty on the trajectories that deviate from the one that is as close to the straight line as possible. Since for the optimal tunnelling trajectory Δy is zero both at t_0 and t_i, we safely neglect the corrections to the Coulomb correction along such trajectory in the further analysis.

During the motion in the continuum after ionization, the second (Coulomb) term in the integrand in Eq.(27) is clearly negligible compared to the first term. Indeed, if $F_{2\omega} = \epsilon F_\omega$, the first term in the integrand scales as $\epsilon^2 U_p$, where $U_p = F_\omega^2/(4\omega^2)$ is the ponderomotive potential in the fundamental field. The second term scales as $\epsilon^2/(16\alpha_\omega)$. Thus, the ratio of the second to the first term scales as $[16U_p\alpha_\omega]^{-1}$, where $\alpha_\omega = F_\omega/\omega^2 \gg 1$ is the electron oscillation amplitude in the strong fundamental field. Since $1/\alpha_\omega \ll I_p$, the second term is completely negligible in the tunnelling regime of $\gamma < 1$.

Thus, we can conclude that the leading term responsible for the modification of the ionization and propagation amplitudes of the electron by the presence of the second color is

given by the gate:

$$G(\Omega,\phi) = \exp\left[-i\frac{1}{2}\int_{t_0}^{t_r} dt''[p_y + A_{2\omega}(t'')]^2\right], \tag{29}$$

where t_0, t_r depend on Ω via the link $\Omega(t_r, t_0)$ for the single-color case and in general include the Coulomb corrections to the SFA expressions Eqs.(23). The dependence on the two-color delay comes from the vector potential $A_{2\omega}(t'')$. A detailed analysis of this gate $G(\Omega,\phi)$ is given in the next section.

The gate Eq.(29) does not yet include the effect of the SH field on the recombination. Namely, the weak control field at the frequency 2ω breaks the symmetry between the two subsequent laser half-cycles, lifting the exact destructive interference for the emission at even harmonic frequencies. Let θ be the small deviation angle of the velocity of the returning electron from x axis, i.e. from the polarization direction of the fundamental field. In atoms, for odd harmonics, the interference of the two subsequent half-cycles leads to the reduction of the harmonic amplitude proportional to $\cos\theta$, whereas for the even harmonics the same interference yields the factor $\sin\theta$. Since the angle of return θ depends on the relative delay ϕ between the two fields, the angle θ works as a velocity gate. For a weak control field, the effect of the velocity gate is very significant for the even harmonics, which are simply absent if $\theta = 0$. For odd harmonics, the effect of $\cos\theta$ is small compared to the exponential gate Eq.(29), in part due to the finite range of alignment angles in the molecular ensemble – the uncertainty in the alignment angle is significantly larger than θ. The same argument does not, of course, apply to even harmonics as their appearance is solely due to $\theta \neq 0$.

In the following we will use Eq.(29) to analyze the effect of the weak SH field on the intensities of odd harmonics.

B. Analysis of the two-color gate

This sub-section gives detailed analysis of the displacement and ionization gate for the case of a single ionization channel correlated to a single state of the ion.

As shown in the previous section, the change in the harmonic emission amplitude introduced by the SH field is given by

$$G(\Omega,\phi) = \exp\left[-i\frac{1}{2}\int_{t_0}^{t_r} dt''[p_y + A_{2\omega}(t'')]^2\right]. \tag{30}$$

The instants t_0 and t_r are linked to the emission frequency Ω. They realize the stationary phase points of the general quantum expression Eq.(21) in the absence of the 2ω field, and are dictated by the electron motion only in the strong fundamental field and the core potential. That is, they include the corrections to the times obtained within the SFA.

The drift momentum p_y that enters the above expression is determined by the stationary phase condition with respect to p_y

$$\frac{\partial}{\partial p_y}\frac{1}{2}\int_{t_0}^{t_r} dt''[p_y + A_{2\omega}(t'')]^2 = \int_{t_0}^{t_r} dt''[p_y + A_{2\omega}(t'')] = 0, \tag{31}$$

which means that the electron trajectory has to return to the vicinity of the core, where the recombination takes place.

The laser field is set as $F(t) = F_\omega \cos\omega t\ \mathbf{e}_x + F_{2\omega}\cos(2\omega t + \phi)\ \mathbf{e}_y$. The vector potential for the SH field is

$$A_{2\omega}(t) = -\frac{F_{2\omega}}{2\omega}\sin(2\omega t + \phi) = -\frac{\epsilon F_\omega}{2\omega}\sin(2\omega t + \phi), \tag{32}$$

where ϵ is the field ratio. Thus, the phase of the gate can be written as

$$S_y = \frac{1}{2}\left[\frac{\epsilon F_\omega}{2\omega}\right]^2 \int_{t_0}^{t_r} dt''[\pi_y - \sin(2\omega t'' + \phi)]^2, \tag{33}$$

where the dimensionless momentum is introduced,

$$p_y = \left[\frac{F_{2\omega}}{2\omega}\right]\pi_y = \left[\frac{\epsilon F_\omega}{2\omega}\right]\pi_y. \tag{34}$$

It is also convenient to change from time variables to dimensionless phases, $\omega t_0 = \varphi_0$, $\omega t_r = \varphi_r$, $\omega t'' = \varphi$, yielding

$$\begin{aligned} S_y &= \frac{1}{2\omega}\left[\frac{\epsilon F_\omega}{2\omega}\right]^2 \sigma(\Omega,\phi) \\ \sigma(\Omega,\phi) &= \int_{\varphi_0}^{\varphi_r} d\varphi[\pi_y - \sin(2\varphi + \phi)]^2, \end{aligned} \tag{35}$$

and for the gate

$$G(\Omega,\phi) = \exp\left[-i\frac{1}{2\omega}\left[\frac{\epsilon F_\omega}{2\omega}\right]^2 \sigma(\Omega,\phi)\right]. \tag{36}$$

Our experiment measures the intensity modulation of the harmonic signal as a function of the two-color delay ϕ. Had the phase $\sigma(\Omega,\phi)$ been purely real, there would have been no modulation within the quantum trajectory formalism. Within this formalism, the modulation arises because the stationary phase point φ_0 is complex, $\varphi_0 = \varphi_i + i\varphi_T$. Its imaginary

part reflects the tunnelling process and its real part φ_i determines the ionization time when the electron is expected to exit the barrier, $\varphi_i = \omega t_i$, $i\varphi_T = i\omega\tau_T$, with $i\tau_T$ referred to as 'tunnelling time'.

Here and below we assume that the recombination times and drift momenta p_x and p_y are real, i.e. we describe harmonics via electrons moving in the real continuum. This assumption is adequate unless the emitted harmonic frequencies are too close to the ionization threshold. For our experimental parameters, the corrections associated with a small imaginary part in t_r are negligible for helium for harmonics above 25.

Due to the presence of the imaginary component $i\varphi_T$ the phase σ also acquires the imaginary component $\mathrm{Im}\sigma$, which is given by the integral from φ_0 to the real axis:

$$\begin{aligned}\mathrm{Im}\sigma(\Omega,\phi) &= \mathrm{Im}\int_{\varphi_i+i\varphi_T}^{\varphi_i} d\varphi[\pi_y - \sin(2\varphi+\varphi)]^2 = \\ &= -\mathrm{Re}\int_0^{\varphi_T} d\varphi[\pi_y - \sin(2\varphi_i + 2i\varphi + \phi)]^2 \end{aligned} \tag{37}$$

This component introduces an amplitude modulation of the harmonic signal. Up to the phase accumulated between t_i and t_r (which is the same for adjacent half-cycles and is therefore insignificant for the many-cycle pulses we use) the gate is

$$G(\Omega,\phi) = \exp\left[-\frac{1}{2\omega}\left[\frac{\epsilon F_\omega}{2\omega}\right]^2 \mathrm{Re}\int_0^{\varphi_T} d\varphi[\pi_y - \sin(2\varphi_i + 2i\varphi + \phi)]^2\right]. \tag{38}$$

The integral in Eq.(38) is quadratic in π_y. Thus, we can re-write it exactly as follows:

$$\mathrm{Re}\int_0^{\varphi_T} d\varphi[\pi_y - \sin(2\varphi_i + 2i\varphi + \phi)]^2 = (\pi_y - \pi_y^{(T)})^2\varphi_T + \mathrm{Re}\int_0^{\varphi_T} d\varphi[\pi_y^{(T)} - \sin(2\varphi_i + 2i\varphi + \phi)]^2, \tag{39}$$

where the optimal tunnelling momentum $\pi_y^{(T)}$ is defined by the equation

$$\frac{\partial}{\partial\pi_y}\mathrm{Re}\int_0^{\varphi_T} d\varphi[\pi_y - \sin(2\varphi_i + 2i\varphi + \phi)]^2 = 0. \tag{40}$$

This equation is simply the requirement that the real part of lateral electron displacement during tunnelling is equal to zero,

$$\mathrm{Re}\int_0^{\varphi_T} d\varphi[\pi_y - \sin(2\varphi_i + 2i\varphi + \phi)] = 0, \tag{41}$$

which yields optimal lateral momentum for tunnelling

$$\pi_y^{(T)}(\phi) = \frac{\sinh(2\varphi_T)}{2\varphi_T}\sin(2\varphi_i + \phi). \tag{42}$$

Calculating the required integral, we obtain the expression for the modulation of the harmonic amplitudes:

$$G(\Omega,\phi)=\exp\left[-\frac{\varphi_T}{2\omega}\left[\frac{\epsilon F_\omega}{2\omega}\right]^2\left[(\pi_y-\pi_y^{(T)}(\phi))^2+g_1(\varphi_T)[\pi_y^{(T)}(\phi)]^2-g_2(\varphi_T)\right]\right] \tag{43}$$

The modulation of the harmonic intensity is given by square of this expression, $G^2(\Omega,\phi)$. The functions $g_1(\varphi_T)$ and $g_2(\varphi_T)$ are

$$\begin{aligned} g_1(\varphi_T)&=\frac{\varphi_T\sinh 4\varphi_T}{\sinh^2 2\varphi_T}-1\\ g_2(\varphi_T)&=\frac{\sinh 4\varphi_T}{4\varphi_T}-1 \end{aligned} \tag{44}$$

We can now analyze the physics encoded into the expression for the gate. First of all, we note that the third (last) term in the exponent is independent of the two-color delay ϕ and therefore does not contribute to the amplitude modulation. It reflects the average enhancement of the ionization rate due to the presence of the second field. The ϕ-dependent modulation is introduced by the first and the second terms in the exponent.

The second term reflects the extra cost associated with the deviation of the optimal tunnelling trajectory from the straight line. This deviation is induced by the control field. The cost is minimal if the lateral momentum $\pi_y^{(T)}(\phi)$ is minimized. Together with the third term, they form the ionization gate

$$G_{\rm ion}(\Omega,\phi)=\exp\left[-\frac{\varphi_T}{2\omega}\left[\frac{\epsilon F_\omega}{2\omega}\right]^2\left[g_1(\varphi_T)[\pi_y^{(T)}(\phi)]^2-g_2(\varphi_T)\right]\right]. \tag{45}$$

The first term in the exponent in Eq.(43) characterizes the tunnelling-imposed relative cost of populating the trajectory with the lateral drift momentum π_y. Recall that π_y is the drift momentum that ensures the return of the trajectory to the core at the correct recombination time t_r. That is, it ensures zero lateral displacement between $\varphi_0=\varphi_i+i\varphi_T$ and φ_r. The amplitude of populating this trajectory is the displacement gate:

$$G_y(\Omega,\phi)=\exp\left[-\frac{\varphi_T}{2\omega}\left[\frac{\epsilon F_\omega}{2\omega}\right]^2\left[(\pi_y-\pi_y^{(T)}(\phi))^2\right]\right] \tag{46}$$

It is maximized if $\pi_y=\pi_y^{(T)}$, i.e. if the same drift momentum also optimizes tunnelling (zero displacement inside the barrier region).

If we restrict the lateral drift momenta and lateral displacements to real values, then π_y is

$$\pi_y=\frac{1}{2(\varphi_r-\varphi_i)}\left[\cosh(2\varphi_T)\cos(2\varphi_i+\phi)-\cos(2\varphi_r+\phi)\right], \tag{47}$$

and the condition $\pi_y = \pi_y^{(T)}$ reads

$$\frac{1}{2(\varphi_r - \varphi_i)} \left[\cosh(2\varphi_T)\cos(2\varphi_i + \phi) - \cos(2\varphi_r + \phi)\right] = \frac{\sinh(2\varphi_T)}{2\varphi_T}\sin(2\varphi_i + \phi). \quad (48)$$

In the tunnelling limit of small φ_T this condition becomes

$$\frac{1}{2(\varphi_r - \varphi_i)} \left[\cos(2\varphi_i + \phi) - \cos(2\varphi_r + \phi)\right] = \sin(2\varphi_i + \phi). \quad (49)$$

The exact same condition is obtained by assuming that the control field only acts on the electron after it exits the barrier at φ_i, and that the electron exits the barrier with zero instantaneous lateral velocity.

Thus, in the tunnelling limit the control field indeed probes the trajectory after it leaves the barrier, and the optimal two-color delay ϕ given by the quantum displacement gate $G_y(\Omega, \phi)$ is the same as that obtained from the simple classical picture. Importantly, the coefficient $g_1(\varphi_T)$ is small in the tunnelling regime of $\gamma \ll 1$, which also ensures that the ionization gate plays a minor role in this regime.

For the actual parameters of our experiment in helium, both classical and quantum reconstruction procedures give very close results, as shown in the paper. Figure 2 (SI) shows the calculated gated signal for helium atoms according to the full quantum mechanical derivation (left panel) and the classical derivation (right panel). As can be seen in the figure, the modifications due to the quantum effects are small.

In order to use the quantum expression for the reconstruction, we first use the semi-classical gate Eq. (49) to obtain the recollision times t_r. We then insert these times into the quantum gate (Eq. 48) together with the experimental phases ϕ^y_{max} and obtain the ionization times t_i. The imaginary part of the ionization times φ_τ are obtained from the imaginary part of the second of Eqs. (23). We confirmed that the corresponding quantum corrections are small (see Fig. 3c in the article).

In the regime of non-adiabatic tunneling $\gamma \sim 1$ the quantum features in the displacement gate (the terms depending on φ_T) and the modifications to the ionization amplitude described by $G_{\rm ion}(\Omega, \phi)$ Eq.(45) must, of course, be included. However, these changes are relatively slow and smooth due to the behavior of $g_1(\varphi_T)$, which is close to unity for $\varphi_T \simeq 1$. The optimal two-color delay remains essentially the same for both the quantum and the semi-classical gates in the case of the CO_2 molecule and 800 nm radiation with intensity $I = 1.3 \times 10^{14}$ W/cm^2.

VII. QUANTUM ORBITS AND THE ROLE OF THE MEASUREMENT IN STRONG FIELD DYNAMICS

Here we compare the similarities and differences between the electron trajectories responsible for high harmonic generation and those associated with strong-field ionization. At first glance, one might think the trajectories describing the motion of the continuum electron are the same as those responsible for high harmonic emission. However, as often the case in quantum mechanics, the specific measurement (observable) has fundamental impact on the characteristics of the relevant trajectories.

In strong-field ionization, when the detached electron is detected, the observable is the electron drift momentum $\mathbf{p}$ after the end of the laser pulse. Obviously, $\mathbf{p}$ must be a real-valued quantity. In high harmonic generation, the observable is the emitted light, with real-valued frequency (photon energy). Other characteristics of the relevant electron trajectories, including their momenta, do not in principle have to be real-valued if they are not measured.

Consider a linearly polarized laser field. The quantum orbits relevant for high harmonic generation are the solutions $(p = p_0, t = t_r, t' = t_0)$ of the following equations:

$$\int_{t_0}^{t_r} [p_0 + A(t')]dt' = 0, \tag{50}$$

$$\frac{[p_0 + A(t_0)]^2}{2} + I_p = 0 \tag{51}$$

$$\frac{[p_0 + A(t_r)]^2}{2} + I_p = \Omega \ . \tag{52}$$

with the perpendicular component of $\mathbf{p}$ equal to zero, $p_\perp = 0$. These equations ensure that the phase $\Sigma(\mathbf{p}, t, t')$

$$\Sigma(\mathbf{p}, t, t') = \frac{1}{2}\int_{t'}^{t} dt'' \left[\mathbf{p} + A(\tau')\right]^2 + I_p(t - t') - \Omega t = S(\mathbf{p}, t, t') + I_p(t - t') - \Omega t \tag{53}$$

that enters the Feynman path integral describing the HHG process [5] is stationary. Eqs.(50,51,52) describe the trajectories which, together with the stationary phase region around them, are responsible for the measured harmonic signal. To simplify the notations and the analysis, we will now drop the perpendicular component of $\mathbf{p}$, which is equal to zero.

In Eqs.(50,51,52), the observable is the energy Ω of the emitted photon, and the solutions must ensure that Ω is real-valued. Obviously, real-valued p_0 and t_r in the equation $[p_0 +$

$A(t_r)]^2/2 + I_p = \Omega$ would fit that last requirement. However, real-valued p_0 and t_r may not satisfy Eqs.(50,51).

Let $t_0 = t_i + i\tau_T$ be the complex-valued moment of ionization. Consider Eq.(50), which describes the electron displacement between t_0 and t_r. Integration from t_0 to the real time axis t_i yields, in general, non-zero imaginary component of the displacement, which we will denote Δ_i. If p_0 and t_r are both real-valued, the remaining integral from t_i to t_r would also be real-valued, unable to compensate the imaginary displacement Δ_i. This is the reason why the quantum orbits have imaginary components both in p_0 and t_r. Note that if p_0 were real, Eq.(52) would force t_r to be real.

Thus, the measurement (observable) leads to differences for the electron trajectories that determine the strong-field dynamics in case of ionization (real observable p) and HHG (real observable Ω). Given these differences, can the information extracted from HHG measurements can be used to understand the dynamics of tunnelling? The answer is 'yes', provided certain conditions are met. What are these conditions?

Mathematically the application of the saddle point method to the Feynman path integrals describing HHG [5] relies on expanding $\Sigma(p, t, t')$ up to the second order around the stationary trajectories given by Eqs.(50,51,52). However, $\Sigma(p, t, t')$ is purely quadratic function of p and hence can be expanded to the second order in p around any other $p = p_1$.

Let us now select this p_1 to be real-valued, and require that it compensates only for the real part of the electron displacement between t_0 and t_r,

$$\mathrm{Re}\int_{t_0}^{t_r}[p_1 + A(t')]dt' = 0, \tag{54}$$

Writing $p_0 = p_1 + \Delta p$ and using Eq.(50) for p_0, the phase Σ can be re-written as

$$\Sigma(p_0, t_r, t_0) = \Sigma(p_1, t_r, t_0) - \frac{1}{2}[\Delta p]^2(t_r - t_0) = \Sigma(p_1, t_r, t_0) - \frac{1}{2}\frac{\Delta_i^2}{t_r - t_0}. \tag{55}$$

Thus, at first glance it looks that one can use real-valued momentum p_1, appropriate for the ionization, as long as one includes the extra term in the phase Σ, which effectively means correction to the electron energy upon return to the nucleus when compared to the time derivative of $\Sigma(p_1, t_r, t_0)$. In other words, one can use the 'photo-electron trajectories', characterized by real-valued momentum p_1, to analyze the trajectories responsible for high harmonic emission, and vice versa – the measurements of high harmonics can be used to analyze the dynamics of ionization.

The important caveat is the change in times t_0 and t_r associated with replacing complex-valued p_0 with real-valued p_1. As explained above, if we replace Eq.(50) with Eq.(54) and keep Eq.(51) and Eq.(52) unchanged, p becomes real-valued and thus t_r is also real-valued due to Eq.(52). The moment of recombination shifts to the real time axis. Thus, the analysis of high harmonic emission in terms of electron trajectories associated with real ionization, i.e. real-valued p, is only possible if the imaginary part of t_r is sufficiently small. Mathematically, $\mathrm{Im}t_r$ should be within the width of the saddle-point region. Similar condition applies to changes in t_0. These requirements are indeed met for all but the shortest trajectories, for our experimental conditions of 800 nm laser wavelength corresponding to the phases of return $\omega t_r \leq (0.3-0.35)\times 2\pi$. The accuracy of the approach can be easily gauged by comparing the phases calculated in both approaches (with the term $\Delta_i^2/(t_r - t_0)$ included). Alternatively, one can compare the time-derivatives of the phases, which is the crucial component for the harmonic emission. This comparison shows that for our experimental conditions the analysis of the harmonic emission in terms of photo-electrons is valid for CO_2 for harmonics above H15-17 at intensities $I \simeq 10^{14}\mathrm{W/cm}^2$, and for helium for harmonics above H25.

VIII. DEFINITIONS OF IONIZATION TIMES IN STRONG FIELD TUNNELING

Mathematically, the classical three-step model of high harmonic generation [19] obtains from Eqs.(50,51,52) by setting $I_p = 0$ in Eq.(51). In this case the moments of ionization and recombination, as well as the drift momentum are purely real, and the electron is 'born in the continuum' at the origin. Clearly, setting $I_p = 0$ in Eq.(51) is an approximation valid only if the energy U_p of electron oscillations in the continuum is very large, $\gamma^2 = I_p/2U_p \ll 1$. Therefore, one might be tempted to conclude that it is by no means surprising when the experimental measurements performed in the regime of $\gamma^2 \approx 0.6$, as in our experiment, find differences from this simple picture.

However, the situation is not nearly as simple. There is absolutely no need to use the approximation $I_p = 0$ in Eq.(51), yet the moment of ionization can still be naturally associated with the moment when the electron velocity is equal to zero. Indeed, the standard model of strong field ionization extends the picture of tunnelling in static electric fields to the case of slowly oscillating laser fields. As the electron tunnels through slowly oscillating barrier, its velocity at the turning point of the semi-classical trajectory – the exit from the

classically forbidden region – is expected to be equal to zero.

There is a crucial difference between this perspective and the simple classical model. In the latter, the electron appears in the continuum not only with zero velocity, but also at the origin. In contrast, in the semi-classical picture the electron emerges from the classically forbidden region offset from the origin, at the turning point of its semi-classical trajectory. The non-zero displacement of the electron at the moment of ionization leads to well known consequences – the increase in the cut-off energy of the harmonic emission [20]. The simple classical model yields $\Omega_{\rm cutoff} = I_p + 3.17U_p$ while the quantum treatment [20] yields $\Omega_{\rm cutoff} \simeq 1.32I_p + 3.17U_p$, with the additional energy of $0.32I_p$ gained by the electron due to this initial displacement, which the electron must now traverse before recombination.

The nearly zero electron velocity at the moment of ionization was explicitly pointed out by Keldysh [21], who introduced the distinction between the tunnelling and multi-photon regimes of strong-field ionization using the exact analogue of the Buttiker-Landauer tunnelling time [22]. Importantly, Ref.[21] stressed that the electron velocity upon ionization is small both in tunnelling and multi-photon regimes. One arrives at the same conclusion about the ionization times by applying the streak-camera principle to the case of strong-field ionization, where it reads $\mathbf{p} = -\mathbf{A}(t_i)$.

Thus, the definition of the ionization time as the moment when the instantaneous electron velocity is equal to zero is not equivalent to setting $I_p = 0$ in Eq.(51). Nevertheless, both in the classical and semi-classical pictures, the ionization times are spread over essentially the same window up to 0.25 laser cycle after each crest of the oscillating field. On the other hand, the times t_i defined as $t_i = \mathrm{Re}(t_0)$ are confined to much more narrow window. Our experimental results are unambiguously consistent with this latter definition.

[1] Dudovich, N. *et al.* Attosecond Temporal Gating with Elliptically Polarized Light. *Physical Review Letters* **97**, 253903 (2006).

[2] Krausz, F. & Ivanov, M. Yu. Attosecond physics. *Review of Modern Physics* **81**, 163 (2009)

[3] Shafir, D. *et al.* Atomic wavefunctions probed through strong-field light-matter interaction. *Nature Physics* **5**, 412 (2009).

[4] Shafir, D. *et al.* Probing the symmetry of atomic wavefunctions from the point of view of

strong field-driven electrons. *New Journal of Physics* **12**, 073032 (2010).

[5] Salières, P. *et al.* Feynman's Path-Integral Approach for Intense-Laser-Atom Interactions. *Science* **292**, 902 (2001).

[6] Ivanov, M. Yu., Brabec, T. & Burnett, N. H. Coulomb corrections and polarization effects in high field high harmonic emission. *Physical Review A* **54**, 742-745 (1996).

[7] Lin, C. D. *et al.* Strong-field rescattering physics - self-imaging of a molecule by its own electrons. *Journal of Physics B* **43**, 122001 (2010).

[8] Frolov, M. V., Manakov, N. L., Sarantseva, T. S. & Starace, A. F. Analytic confirmation that the factorized formula for harmonic generation involves the exact photorecombination cross section. *Physical Review A* **83**, 043416 (2011).

[9] Frolov, M. V. *et al.* Analytic Description of the High-Energy Plateau in Harmonic Generation by Atoms: Can the Harmonic Power Increase with Increasing Laser Wavelengths? *Physical Review Letters* **102**, 243901 (2009).

[10] for review, see Popov, V. S. Tunnel and multiphoton ionization of atoms and ions in a strong laser field (Keldysh theory). *Physics - Uspekhi* **47**, 855-885 (2004).

[11] Smirnova, O., Spanner, M. & Ivanov, M. Yu. Coulomb and polarization effects in laser assisted XUV ionization. *Journal of Physics B* **39**, s323 (2006).

[12] Smirnova, O. *et al.* Coulomb-laser coupling in strong-field assisted photoeffect and molecular tomography. *Journal of Physics B* **40**, F197 (2007).

[13] Nagele, S. *et al.* Time-resolved photoemission by attosecond streaking: extraction of time information. *Journal of Physics B* **44**, 081001 (2011).

[14] Zhang, C. H. & Thumm, U. Electron-ion interaction effects in attosecond time-resolved photoelectron spectra. *Physical Review A* **82**, 043405 (2010).

[15] Smirnova, O., Spanner, M. & Ivanov, M. Yu. Analytical solutions for strong field-driven atomic and molecular one- and two- electron continua and applications to strong-field problems. *Physical Review A* **77**, 033407 (2008).

[16] Volkova, E., Gridchin, V., Popov, A. M. & Tikhonova, O. Tunneling ionization of a hydrogen atom in short and ultrashort laser pulses. *JETP* **102**, 40-52 (2006).

[17] Popruzhenko, S. V., Mur, V. D., Popov, V. S. & Bauer, D. Strong Field Ionization Rate for Arbitrary Laser Frequencies. *Physical Review Letters* **101**, 193003 (2008); Tian-Min Yan, Popruzhenko, S. V., Vrakking, M. J. J.& Bauer, D. Low-Energy Structures in Strong Field

Ionization Revealed by Quantum Orbits *Physical Review Letters* **105**, 253002 (2010).

[18] Huismans, Y. *et al.* Time-resolved holography with photoelectron waves. *Science* **331**, 61-64 (2011).

[19] Corkum, P. B. Plasma perspective on strong field multiphoton ionization. *Physical Review Letters* **71**, 1994-1997 (1993).

[20] Lewenstein, M., *et al.* Theory of high-harmonic generation by low-frequency laser fields. *Physical Review A* **49**, 2117 (1994).

[21] Keldysh, L. V. Ionization in the field of a strong electromagnetic wave. *Soviet Physics JETP* **20**, 1307-1314 (1965).

[22] Buttiker, M. & Landauer, R. Traversal Time for Tunneling. *Physycal Review Letters* **49**, 1739-1742 (1982).